Effect of Chromium Substitution on the Local Structure and Insertion Chemistry of Spinel Lithium Manganates: Investigation by X-ray Absorption Fine Structure Spectroscopy

Brett Ammundsen,*,† Deborah J. Jones, and Jacques Rozière

Laboratoire des Agrégats Moléculaires et Matériaux Inorganiques (LAMMI), ESA 5072 CNRS, Université Montpellier 2, Place Eugène Bataillon, 34095 Montpellier Cédex 5, France

Françoise Villain

Laboratoire pour l'Utilisation du Rayonnement Électromagnétique (LURE), Université Paris-Sud (XI), 91405 Orsay Cédex, France

Received: March 18, 1998; In Final Form: June 16, 1998

Chromium substitution in lithium manganate spinels of composition $LiCr_xMn_{2-x}O_4$ ($0.2 \leq x \leq 1.0$) is investigated with regard to lithium extraction and insertion reactions. The local structural environments and electronic states of chromium and manganese in the compounds following these reactions have been probed by X-ray absorption near-edge structure (XANES) and extended fine structure (EXAFS) spectroscopies at the Cr and Mn K edges. The data show that the replacement of d^4 Mn^{3+} ions by d^3 Cr^{3+} in the octahedral framework of the spinels eliminates the local disorder present in the lattice around $[Mn^{3+}O_6]$ octahedra, which are distorted by Jahn−Teller stabilization of the electronic state. Reversible extraction and sorption of lithium, in HCl and LiOH solutions, respectively, take place with changes in the oxidation state of Mn. The Cr remains stable as the trivalent species for HCl concentrations ≤ 0.5 M. Additional insertion of lithium in $LiCr_xMn_{2-x}O_4$ by reaction with butyllithium produces tetragonal $Li_2Cr_xMn_{2-x}O_4$ spinels, but the degree of tetragonal distortion is significantly reduced by Cr substitution. The XAFS data show that while the $[Mn^{3+}O_6]$ octahedra in the tetragonal phases are elongated along one axis, $[Cr^{3+}O_6]$ octahedra retain a regular symmetry with six equal Cr−O distances.

Introduction

Spinel lithium manganates are lithium and proton insertion compounds with technological applications as lithium-selective ion sieves[1−8] and as cathode materials in rechargeable batteries.[9−16] The insertion properties and structural characteristics are highly sensitive to the precise stoichiometry of the compounds, particularly oxygen content and the oxidation state of the manganese ions, which are highly variable.[1,7,17−19] This diversity and complexity of structure−property relationships have led to a tremendous amount of both fundamental and applied research concerned with the effects of preparation conditions on the oxidation−reduction and ion-exchange characteristics of the compounds.[1−7,20−29]

Recently there has been a growing interest in the substitution of a fraction of the manganese as a means of tailoring the insertion properties of lithium manganates.[30−32] In particular, the substitution of Mn^{3+} in the mixed-valence Mn^{3+}/Mn^{4+} spinel $LiMn_2O_4$ by other trivalent ions of the transition element series has been explored to improve the cyclability in applications as cathode materials.[32,33] However, while many of the studies so far published have examined the bulk structural characteristics and electrochemical properties of substituted manganates, very little is known about the local structures of the compounds.

We present here a detailed investigation of the effects of chromium substitution for manganese in the spinel system $LiCr_xMn_{2-x}O_4$, $0.2 \leq x \leq 1$. A number of studies have shown that chromium substitution in $LiMn_2O_4$ results in better cyclability and reduced capacity fading in lithium batteries, and therefore gives a corresponding improvement in rechargeability.[33−35] This increased stability over many cycles has been attributed to a better reversibility of the changes in crystal structure which occur during insertion and extraction of lithium ions.[33,34] In one study, chromium substitution was furthermore shown to increase the specific capacity and energy when voltages of >4.9 V were applied to remove lithium ions in the charging cycle.[36] Faster lithium diffusion has also been measured in chromium-substituted spinels compared with $LiMn_2O_4$.[37,38]

The presence of a heteroatom such as chromium is expected to influence also the insertion properties of the compounds in aqueous solutions. Lithium manganates undergo lithium extraction and insertion in aqueous solutions by both redox mechanisms and lithium-proton exchange.[7,27] The redox mechanism of lithium extraction in acidic solution involves disproportionation of lattice Mn^{3+} to Mn^{2+} and Mn^{4+},[39] but the disadvantage for applications as a cyclable sorption material is that this results in some dissolution of the compound as the Mn^{2+} ions are released into solution.[6] Lithium manganates which exchange lithium for protons are characterized by a low content of Mn^{3+} ions,[7,25−27] which suppresses the disproportionation process and consequently eliminates the problem of dissolution. However, the resulting delithiated spinels have highly cation-defective structures and contain structural water which appears to limit the reexchange of the protons for lithium.[25,26] It might therefore

† Also affiliated to the School of Chemical and Physical Sciences, Victoria University of Wellington, P.O. Box 600, Wellington, New Zealand.

S1089-5647(98)01549-1 CCC: $15.00
Published on Web 09/22/1998

be useful to substitute a trivalent metal ion which could lower the Mn^{3+} content on the one hand but stabilize the spinel octahedral framework structure on the other.

In the present work, we correlate the insertion properties of chromium-substituted lithium manganates with the local structure determined by X-ray absorption spectroscopy. We have recently shown that X-ray absorption near-edge structure (XANES) and extended fine structure (EXAFS) can provide unique insights into the local structural and electronic effects of lithium insertion on the manganese oxide framework of spinel lithium manganates, following the changes induced by both redox reactions and lithium-proton exchange.[27,40] The technique is particularly well adapted to examining the local structural and electronic effects of substitutional atoms in an insertion compound because the local environments of different elements can be probed separately, allowing the structure to be determined with respect to each of the individual components.

Experimental Section

Samples. Chromium-substituted lithium manganates were prepared by grinding Cr_2O_5, obtained by decomposition of Cr_2O_3 (Aldrich) at 340 °C,[41] with stoichiometric mixtures of $LiNO_3$ and γ-MnO_2 (Aldrich) in acetone to give fine homogeneous powders. The mixtures were fired at 400 °C in air for 5 h, reground, fired at 400 °C in air for another 15 h, reground, and then fired for a further 30 h in air at a final temperature between 400 and 700 °C. Stoichiometric $LiMn_2O_4$ was prepared by heating a mixture of Li_2CO_3 and $MnCO_3$ at 800 °C in air for 24 h, and $Li_{1.33}Mn_{1.67}O_4$ by heating a mixture of Li_2CO_3 and $MnCO_3$ at 400 °C in air for 8 h. $LiCrO_2$ was prepared by heating a mixture of $LiNO_3$ and Cr_2O_5 at 550 °C in air for 48 h, followed by heating at 800 °C in air for 72 h. Compounds were leached in 0.5 M and 1 M HCl by stirring the powders in the acid solutions for 72 h. Lithium sorption in the acid-leached samples was achieved by stirring in 0.1 M solutions of LiOH for 72 h. Lithium insertion in $LiCr_xMn_{2-x}O_4$ using butyllithium was carried out by saturating the powders in 6 M butyllithium solutions in hexane (Aldrich) for 72 h at room temperature, in a dried glovebox filled with nitrogen.

Sample Characterization. Lithium, chromium, and manganese contents were determined by flame spectrometry after dissolution of the samples in hot concentrated sulfuric acid and hydrogen peroxide. Quantities of lattice water in the acid-leached compounds were estimated from the sample weight losses between 100 and 250 °C,[7,25] measured using a Stanton Redcroft STA-781 series thermal analyzer. Powder X-ray diffraction (XRD) patterns were recorded with Cu Kα radiation using an automated Philips diffractometer. Phase identification and evaluation of lattice parameters were carried out from the powder XRD patterns using the Rietveld refinement program FULLPROF.[42]

X-ray Absorption Measurements. X-ray absorption spectra were recorded at the Cr and Mn K-edges in transmission mode on the EXAFS 3 spectrometer at the French synchrotron facility DCI at LURE, using Si [311] (XANES) and [111] (EXAFS) double monochromators slightly detuned for harmonic rejection. Samples were diluted in boron nitride powder and prepared as Nujol mulls pressed between the Parafilm windows of steel holders, and maintained at 77 K in a cold-finger cryostat. XANES spectra were recorded in a 0.3 eV step size, and EXAFS spectra in a 1.5 eV step size to 900 eV after the absorption edge. In the case of the Cr-substituted lithium manganates, the EXAFS data at the Cr K-edge were limited to 500 eV after the absorption edge (ca. 6000 eV) due to the onset of Mn absorption at ca. 6540 eV. Energy calibration was carried out prior to all measurements using 10 μm Cr and Mn foils.

Data were analyzed using the XAS programs of Michalowicz.[43] EXAFS spectra were normalized in the $\mu_{1,\mathrm{exp}} - \mu_{0,\mathrm{exp}}$ convention after simulating the atomic absorption $\mu_{0,\mathrm{exp}}$ with third-order polynomials or spline functions. Fourier transformations using a Kaiser apodization window ($\tau = 3.5$) were performed over the k range 2.5−15 Å^{-1} (2.5−11.5 Å^{-1} for Cr spectra in the substituted manganates) using k^3 weighting.

Distances R_i of the ith shell of atoms from the absorbing atom, and Debye−Waller factors σ_i, were determined using curve-fitting procedures in k space after Fourier filtering to isolate the EXAFS signal $\chi(k)$ corresponding to the relevant maxima in the Fourier transformed data. Theoretical curves were simulated using functions for the backscattering amplitude $F_i(k)$, total phase shift $\phi_i(k)$, and photoelectron mean free path $\lambda(k)$ calculated by the ab initio XAS code FEFF7.[44] The coordination numbers N_i for each shell were fixed to crystallographic values, and the amplitude reduction factor S_0^2 was scaled to a fixed value of 0.86 after preliminary refinements. Only very small adjustments for the energy origin E_0 ($1 < \Delta E_0 < 4$ eV) were then required to optimize the fits of the theoretical data to the experimental data. In all cases the agreement between experimental and theoretical curves gave statistical residues of less than 2% (residue $= \sum_k(k[\chi_{\mathrm{exp}}(k)] - k[\chi_{\mathrm{th}}(k)])^2k^3/\sum_k(k[\chi_{\mathrm{exp}}(k)]^2)$-$k^3$).

Ab initio curved-wave multiple scattering XANES $\mu(E)$ spectra were computed by FEFF7 for atom clusters extending out to ca. 9 Å radius from the central absorbing atom. The Hedin−Lundqvist self-energy was used for the photoelectron, introducing a 1 eV correction to the imaginary part to model the effects of experimental resolution. Paths up to the fourth scattering order and effective radius 9 Å were included in the calculations. Using the approach described by Farges et al.,[45] the filters used to eliminate scattering paths contributing only small amplitudes over the full XAFS range were switched off in order to model the structure in the absorption edge.

Results and Discussion

I. Compositions and Structural Characteristics of the Chromium-Substituted Lithium Manganates. The formation of chromium-substituted lithium manganates was initially investigated for both $LiMn_2O_4$ and $Li_{1+x}Mn_{2-x}O_4$ ($x \leq 0.33$) spinel types. XRD patterns corresponding to single phase cubic spinels were obtained for preparations with Li/(Cr + Mn) ratios of 0.5 and a Cr/Mn ratio of up to 1 at temperatures as low as 400 °C. However, although including Cr_2O_5 as a reactant produced spinels which were more crystalline in XRD than products with lithium and manganese only, as observed previously,[37] leaching of samples prepared at 400 °C in 0.5 M HCl resulted in loss of Cr and the appearance of broad XRD peaks corresponding to formation of some ϵ-MnO_2 phase. A temperature of 600 °C was necessary to obtain products which showed neither loss of Cr nor evidence of structural degradation in 0.5 M HCl. On the other hand, preparations with Li/(Cr + Mn) ratios > 0.5 showed two cubic spinel phases in XRD, and some formation of Li_2MnO_3. One of these spinel phases had relatively broad peaks and a unit cell parameter of ca. 8.15 Å, characteristic of $Li_{1+x}Mn_{2-x}O_4$ compounds.[19,25] The other spinel phase gave sharper XRD lines and a unit cell parameter of ca. 8.20 Å, which corresponds to the Cr-substituted $LiMn_2O_4$ compounds prepared at the same temperature. The results indicate that Cr ions were concentrated in the $LiMn_2O_4$ type phase in preference to the Li-rich phase. Similar results were

TABLE 1: Unit Cell Parameters (a_0) and Chemical Compositions of the Cr-Substituted Lithium Manganates Prepared at 600 °C

x in $LiCr_xMn_{2-x}O_4$	chemical composition	a_0
0.2	$Li_{0.99}Cr_{0.22}Mn_{1.78}O_4$	8.209(3)
0.5	$Li_{1.03}Cr_{0.52}Mn_{1.48}O_4$	8.196(5)
1.0	$Li_{0.97}Cr_{1.01}Mn_{0.99}O_4$	8.192(4)

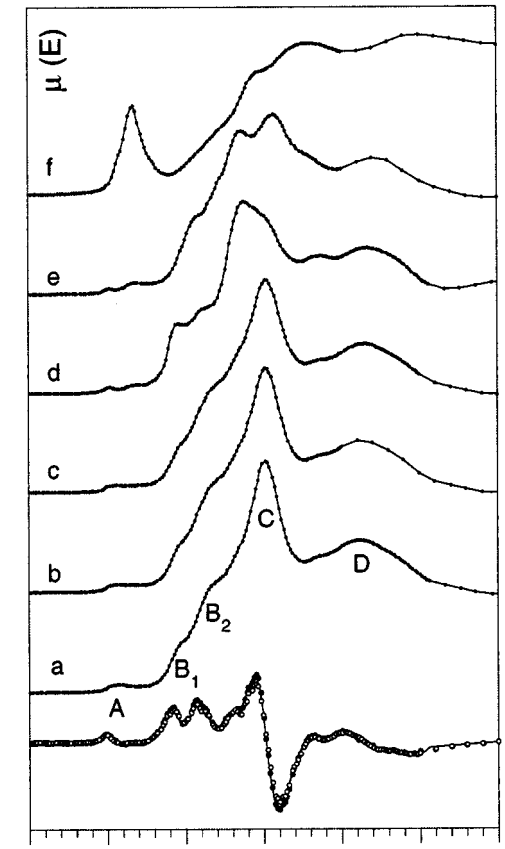

Figure 1. Cr K-edge XANES spectra and first derivatives (below) of $LiCr_xMn_{2-x}O_4$ spinels: (a) $x = 0.2$ (solid line), (b) $x = 0.5$ (dots), (c) $x = 1$ (open circles), compared with XANES spectra of (d) $LiCrO_2$, (e) Cr_2O_3, and (f) CrO_3.

obtained using Li and Mn carbonates as an alternative to $LiNO_3$ and γ-MnO_2.

The compounds selected for more detailed chemical and structural characterization were therefore those having $LiCr_x$-$Mn_{2-x}O_4$ stoichiometry prepared at 600 °C, with compositions $x = 0.2$, 0.5, and 1.0. Refinement of the powder XRD profiles indicated that all these samples were single-phase spinels with the space group *Fd*3*m* in which the chromium and manganese ions reside at the octahedral 16d sites. The chemical compositions and unit cell parameters of these products are given in Table 1. The trend of decreasing unit cell parameter with increasing Cr substitution is well-known and attributed to the replacement of Mn^{3+} ions by a trivalent species having a smaller ionic radius.[30,33,34]

The Cr K-edge X-ray absorption spectra of the three Cr-substituted lithium manganates are shown together with spectra of $LiCrO_2$, Cr_2O_3, and CrO_3 in Figure 1. In Figure 2 the Mn K-edge spectra of the three substituted spinels are compared with spectra of the spinels $LiMn_2O_4$ and $Li_{1.33}Mn_{1.67}O_4$, which have Mn oxidation states ca. 3.5 and 4, respectively.[27] The near-edge structures for the spinel compounds are essentially identical

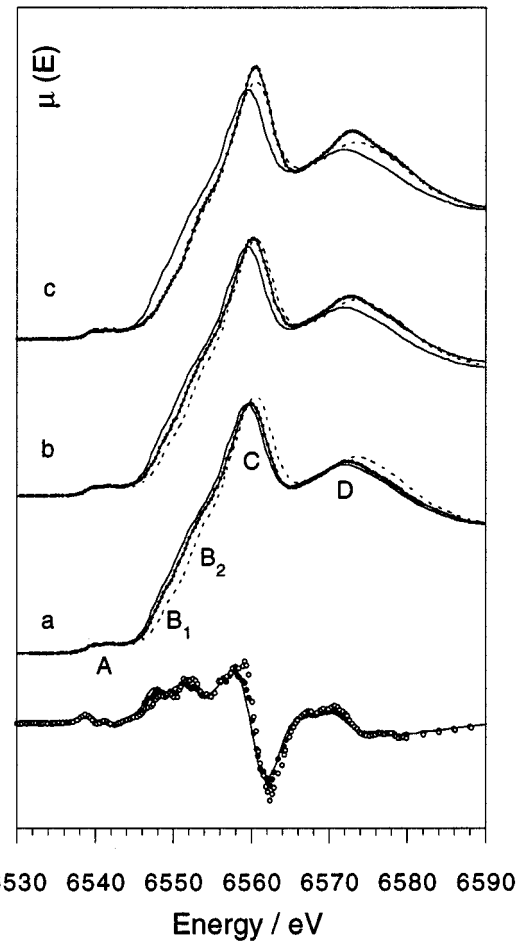

Figure 2. Mn K-edge XANES spectra and first derivatives (below) of $LiCr_xMn_{2-x}O_4$ spinels: (a) $x = 0.2$ (solid line), (b) $x = 0.5$ (dots), (c) $x = 1$ (open circles), compared in each case with XANES spectra of $LiMn_2O_4$ (solid line) and $Li_{1.33}Mn_{1.67}O_4$ (dashed line).

at the Cr and Mn edges, agreeing with the XANES predicted by the ab initio multiple scattering calculations for Cr and Mn in the octahedral 16d site shown in Figure 3. In both calculated and experimental spectra, two steps are present in the absorption edge (labeled B_1 and B_2 in Figures 1−3): there is a relatively intense and symmetric resonance above the absorption edge (C), and a broader structure to higher energy (D). These features are characteristic of the spinel octahedral site, and notably different from the Cr XANES of the layered phase $LiCrO_2$ (Figure 1d), confirming that Cr is fully incorporated into the manganate spinel structures.

The energy positions of the Cr absorption edges are invariant with the degree of substitution in the manganates. The spectra all show a low-intensity preedge feature A, characteristic of the ca. O_h CrO_6 octahedra of trivalent Cr ions (cf. the spectra of $LiCrO_2$ and Cr_2O_3). There is no evidence for the presence of enhanced intensity preedge features as would be expected for asymmetric (T_d or five-coordinate) sites associated with higher Cr oxidation states[46] as observed, for example, for CrO_3 (Figure 1f).

In the Mn spectra, the absorption edges are shifted to higher energy with increasing Cr substitution. This shift is correlated with an increase in Mn oxidation state as a result of Cr substitution, as expected if Cr ions replace trivalent Mn ions to give compounds of composition $LiCr^{3+}{}_xMn^{3+}{}_{1-x}Mn^{4+}O_4$. There is also a narrowing and increase of intensity in the XANES resonances C and D when the degree of Cr substitution is raised. This phenomenon has also been observed during oxidation of

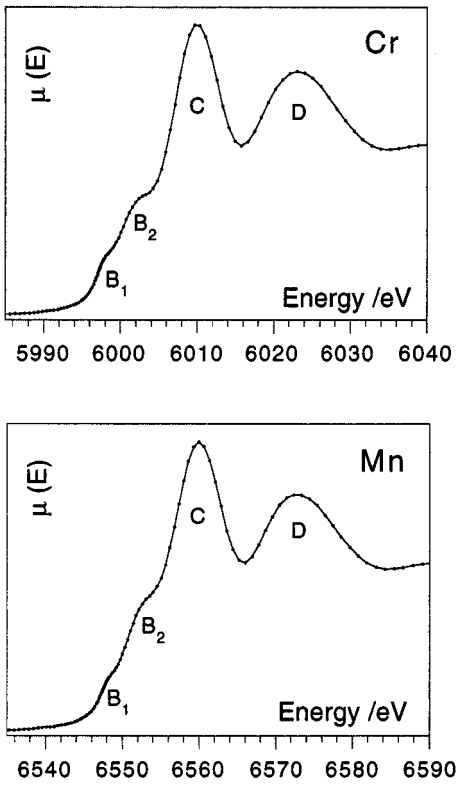

Figure 3. Ab initio calculated K-edge XANES spectra for Cr and Mn atoms in the octahedral 16d site of $LiMn_2O_4$ spinel.

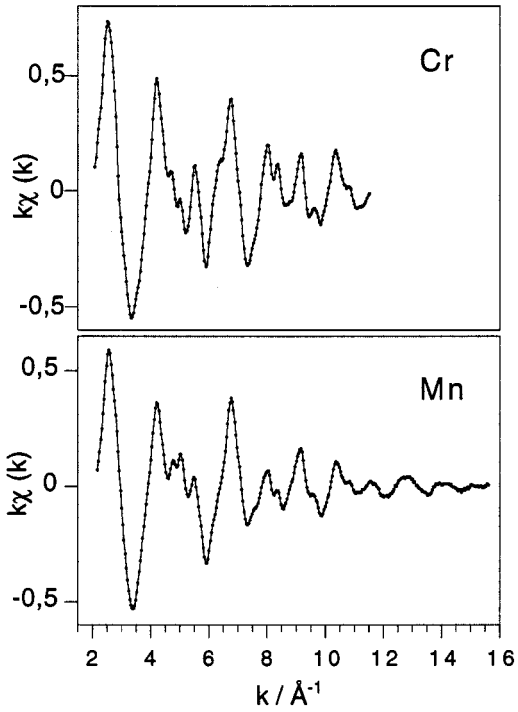

Figure 4. Cr and Mn K-edge EXAFS spectra of $LiCr_{0.5}Mn_{1.5}O_4$.

$LiMn_2O_4$[27] and is associated with increased order in the local structure due to the removal of contributions from Mn^{3+} ions.

EXAFS spectra at the Cr and Mn K-edges are shown in Figure 4 for the $x = 0.5$ compound, and the Fourier-transformed Cr and Mn spectra for all three Cr-substituted lithium manganates are shown in Figure 5. The first two intense peaks in the Fourier-transformed data result from simple backscattering of the photoelectron from the first coordination shell of six oxygen atoms and the shell of cations occupying the six neighboring

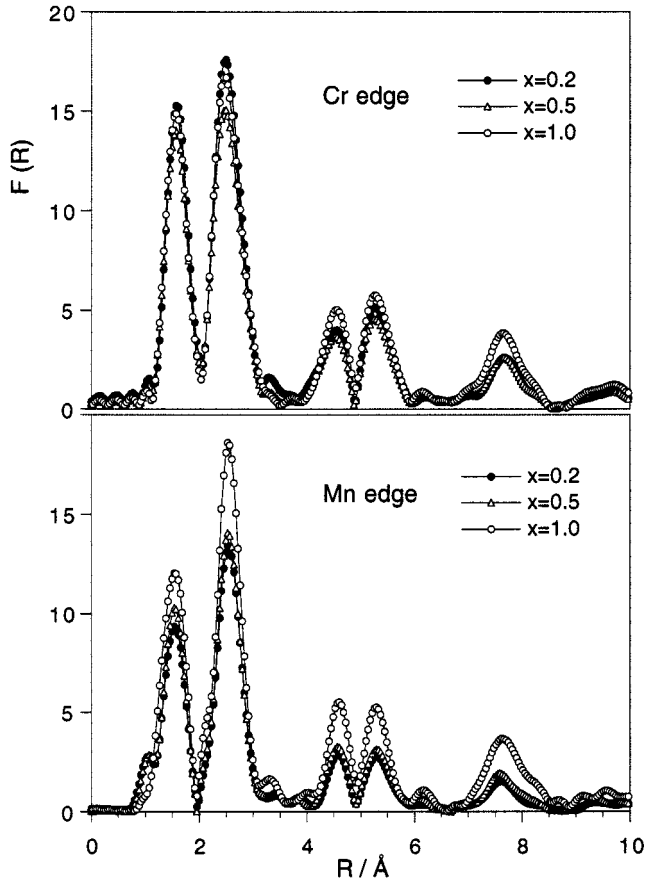

Figure 5. Fourier transformed Cr and Mn EXAFS data for the $LiCr_xMn_{2-x}O_4$ spinels.

16d octahedral sites.[27] Peaks at $R > 4$ Å result from both simple and multiple scattering involving more distant octahedral site cations.[40] Accurate structural information concerning the nearest oxygen and cation neighbors can be obtained by curve-fitting a simple single-scattering model to the experimental data Fourier-filtered over the first two peaks in the transformation.[27] Typical fits to the Cr and Mn data are shown in Figure 6 for the $x = 0.5$ compound. Interatomic distances and Debye−Waller factors determined by this procedure are given in Table 2 for the Cr-substituted spinels, compared with data for $LiMn_2O_4$ and $LiCrO_2$.

For all samples the data for the first coordination shell around both Cr and Mn ions was fitted with six oxygen atoms, in agreement with the expected octahedral site. The Cr−O distances in the spinels, ca. 1.98 Å, are close to those determined for $LiCrO_2$, and essentially invariant with the degree of Cr substitution. The Cr−O Debye−Waller factors are notably smaller than those for Mn−O, and significantly lower in the spinels than in $LiCrO_2$, indicating a high degree of regularity for the CrO_6 octahedron in the three-dimensional spinel framework. The Mn−O distances are ca. 1.91 Å in the Cr-substituted spinels, shorter than the Cr−O distances in the same compounds. In crystalline oxides Mn^{4+}−O distances are typically ca. 1.90 Å, while Jahn−Teller stabilization of the electronic state of high-spin octahedral Mn^{3+} ions generally produces four short Mn^{3+}−O bonds of ca. 1.90 Å and two long Mn^{3+}−O bonds of ca. 2.3 Å. Contributions from the longer Mn^{3+}−O distances manifest primarily as damping of the oscillations in the EXAFS due to incoherence in the photoelectron waves, producing a Fourier transformed peak of reduced intensity and higher Debye−Waller factors in the numerical analysis. The removal of contributions from Mn^{3+} ions when

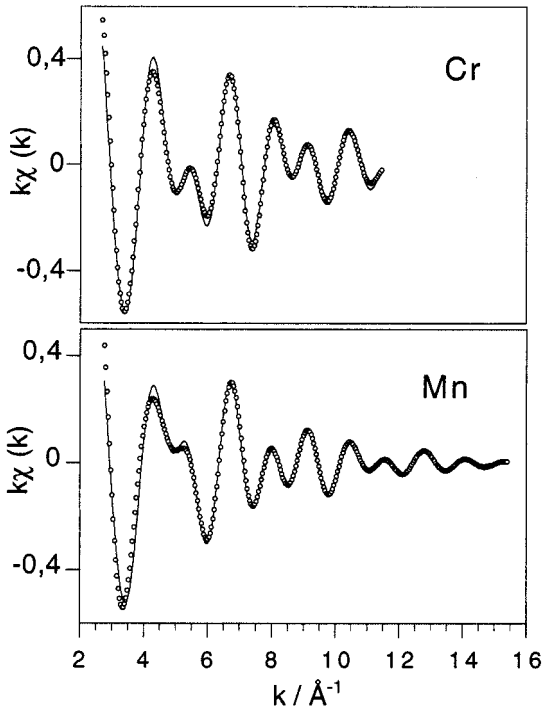

Figure 6. Curve fits (solid lines) to the Cr and Mn EXAFS data (circles) for $LiCr_{0.5}Mn_{1.5}O_4$ filtered over the first two peaks of the Fourier transformations.

TABLE 2: Structural Parameters from EXAFS of the Cr-Substituted Lithium Manganates Prepared at 600 °C

$LiCr_x$-$Mn_{2-x}O_4$	Mn−O		Cr−O		Mn−M		Cr−M	
	R (Å)	σ (Å)	R (Å)	σ (Å)	R (Å)	σ (Å)	R (Å)	σ (Å)
$x = 0.2$	1.908	0.071	1.986	0.039	2.894	0.070	2.892	0.052
$x = 0.5$	1.906	0.065	1.983	0.047	2.887	0.067	2.890	0.062
$x = 1.0$	1.910	0.056	1.976	0.041	2.881	0.054	2.885	0.055
$LiMn_2O_4$[a]	1.925	0.080			2.904	0.074		
$LiCrO_2$			1.993	0.054			2.892	0.063

[a] Parameters taken from ref 27.

the Cr level is increased is seen in the data as a marked decrease in the Debye−Waller factors for the Mn−O shell.

Coordination numbers for the Cr−M and Mn−M shells were fixed to 6, the value expected if all octahedral 16d sites in the spinels were occupied. The Cr−M distances are identical to the Mn−M distances determined for each compound, consistent with homogeneous occupation of the 16d sublattice by Mn and Cr ions. At low levels of substitution, lower Debye−Waller factors are calculated for the Cr−M shell than for the Mn−M shell, indicating a higher degree of cation ordering around the Cr ions than around the Mn ions. This can be attributed to the fact that, unlike tetragonally distorted $[Mn^{3+}O_6]$ octahedra, the $[Cr^{3+}O_6]$ octahedra do not induce distortions in the surrounding local lattice structure. The Debye−Waller factors for the Mn−M shell follow the same trend with Cr substitution as those for the Mn−O shell, converging to the same value as those for the Cr environment as Cr substitution is increased to $x = 1$, when Mn^{3+} is no longer present.

II. Lithium Extraction and Sorption. The compositions and unit cell parameters of the Cr-substituted compounds following leaching in 0.5 M and 1 M HCl are summarized in Table 3. In 0.5 M HCl, which removes >90% of the lithium from $LiMn_2O_4$,[27] Cr substitution resulted in a decrease in the amount of lithium extracted. In nonsubstituted lithium manganates, the amount of Mn^{3+} in the compound determines the amount of lithium that can be extracted in acid by the disproportionation mechanism.[5−7,39] For the Cr-substituted $LiMn_2O_4$ compounds, the reaction can be formulated:

$$Li[Cr_x^{3+}Mn_{(1-x)}^{3+}Mn^{4+}]O_4 + 2(1-x)H^+(aq) \rightarrow Li_x[Cr_x^{3+}Mn^{4+}_{\{1+(1-x)/2\}}]O_{(3+x)} + \{(1-x)/2\}Mn^{2+}(aq) + (1-x)Li^+(aq) + (1-x)H_2O \quad (1)$$

However, the increase in Cr/Mn ratio predicted by reaction 1 was not observed experimentally. The loss of Mn^{2+} occurs from the surface of the solid, and therefore it is likely that some Cr^{3+} ions also pass into solution as the surface dissolves, maintaining the overall Cr/Mn ratio in the solid. The amount of Li remaining in the $x = 0.2$ and $x = 0.5$ compounds after leaching in 0.5 M acid was then only a little higher than that expected if reaction 1 had gone to completion.

An alternative mechanism of lithium extraction in acid solution, often observed for lithium manganate spinels containing small quantities of Mn^{3+}, is by exchange with protons.[7,25−27] Nonsubstituted lithium manganates compensate for the higher Mn^{4+} content by manganese vacancies in the octahedral framework, which allow proton diffusion into the lattice.[26,28,29] Thermogravimetric data for the Cr-substituted spinels showed ≤1% by mass of lattice water after leaching in 0.5 M HCl, indicating that the degree of lithium-proton exchange was low. This low level of proton insertion in the Cr-substituted compounds is probably due to a negligible amount of cation vacancies on 16d octahedral sites.

For the $x = 1.0$ compound $LiCrMnO_4$, the dominant process occurring in 0.5 M or 1 M HCl appeared to be surface dissolution. No variation in the XRD pattern or in the unit cell parameter was observed after acid leaching, suggesting that the bulk crystal structure was essentially unaffected. The dissolution of the surface in this case can be attributed to activation of a Cr oxidation/Mn reduction process such as that described by Manceau et al.,[48] with release of Mn^{2+} and $HCrO_4^-$ ions into solution.

Increasing the acid concentration to 1 M led to increased lithium extraction from the $x = 0.2$ and $x = 0.5$ compounds but was also accompanied by the appearance of chromate ions in the solution. An overall decrease in the Cr/Mn ratios in the remaining solids suggests that Cr loss in this case was not restricted to surface dissolution but resulted at least partly from diffusion out of the bulk. Diffusion of Cr ions out of the octahedral framework would be possible if the Cr ions were oxidized to the +6 state in response to strong positive charging at the surface of the compound resulting from proton binding to surface oxygens. As Cr ions are leached out of the bulk, some proton diffusion into the lattice would be expected for charge compensation. Thermogravimetric analysis indeed indicated an increase in lattice water content for both the $x = 0.2$ and $x = 0.5$ compounds after leaching in 1 M HCl. The infrared spectra of these compounds showed a small absorption peak at 910 cm^{-1}, which is characteristic of of lattice hydroxyl groups in protonated spinel manganese dioxide.[25,26] Recent work indicates that hydroxyls in the MnO_2 spinel framework form at octahedral vacancies.[28,47]

As lithium was extracted from the $x = 0.2$ and $x = 0.5$ compounds, XRD showed both contraction of the lattices, and, for intermediate levels of lithium extraction, splitting of the diffraction lines associated with the presence of two cubic spinel lattices having slightly different lattice parameters. Similar observations for $LiMn_2O_4$ have been attributed to the formation of a stable ordered intermediate $Li_{0.5}Mn_2O_4$ phase with $a_0 =$

TABLE 3: Compositions[a] and Unit Cell Parameters[b] of the Cr-Substituted Lithium Manganates Following Leaching in 0.5 M and 1 M HCl, and after Lithium Sorption in 0.1 M LiOH of the Compound Leached in 0.5 M HCl

$LiCr_x$-$Mn_{2-x}O_4$	leached 0.5 M HCl	lattice water	a_0	leached 1.0 M HCl	lattice water	a_0	after Li sorption	a_0
$x = 0.2$	$Li_{0.34}Cr_{0.22}Mn_{1.78}O_4$	$0.10H_2O$	8.117(4), 64% 8.058(6), 36%	$Li_{0.21}Cr_{0.19}Mn_{1.78}O_4$	$0.24H_2O$	8.104(5), 47% 8.054(5), 53%	$Li_{0.84}Cr_{0.22}Mn_{1.78}O_4$	8.212(4)
$x = 0.5$	$Li_{0.65}Cr_{0.52}Mn_{1.48}O_4$	$0.08H_2O$	8.162(5)	$Li_{0.37}Cr_{0.41}Mn_{1.48}O_4$	$0.17H_2O$	8.151(6), 69% 8.077(7), 31%	$Li_{0.86}Cr_{0.52}Mn_{1.48}O_4$	8.199(6)
$x = 1.0$	$Li_{0.86}Cr_{1.01}Mn_{0.97}O_4$	$0.01H_2O$	8.192(3)	$Li_{0.68}Cr_{1.01}Mn_{0.66}O_4$	$0.02H_2O$	8.191(2)		

[a] Spinel compositions are normalized with [Cr + Mn] ≤ 2, set to the highest value without increasing either the Mn or the Cr stoichiometry above the value of the parent compound. [b] Where two phases were observed by XRD, the percentages of each phase contributing to the diffraction are given as estimated by the Rietveld refinement.

ca. 8.15 Å.[5,7,13,20,24] Slow step voltammetry measurements on Cr-substituted lithium manganate spinels have shown that the disorder−order transition which occurs when the $Li_{0.5}Mn_2O_4$ phase is formed is not perturbed by the presence of Cr^{3+} in octahedral sites.[32,33,38] It is therefore not surprising to observe two-phase behavior for the Cr-substituted spinels here. Figure 7 shows the evolution of the spinel [400] peak in XRD of the $x = 0.2$ and 0.5 compounds. The $x = 0.2$ compound after leaching in 0.5 M acid shows both a phase with $a_0 = 8.12$ Å and a phase with $a_0 = 8.06$ Å. These can be assigned to domains of $Li_{0.5}Cr_{0.22}Mn_{1.78}O_4$ and more completely delithiated "λ"-$Cr_{0.22}Mn_{1.78}O_4$, respectively. Further leaching of lithium in 1 M acid increased the quantity of phase with the lower cell parameter. In the $x = 0.5$ compound, 0.5 M acid gave a single-phase compound with $a_0 = 8.16$ Å. Leaching in 1 M acid then reduced the lithium content below 0.5, giving rise to domains of 8.15 and 8.08 Å phases.

In 0.1 M LiOH solution, the $x = 0.2$ and $x = 0.5$ compounds treated in 0.5 M acid sorbed lithium ions up to compositions of 85−90% the lithium content of the original parent compounds. These Cr-substituted spinels therefore show the same behavior in LiOH solution as lithium-extracted $LiMn_2O_4$, which reinserts lithium back into the original 8a sites in the reaction:[5,6]

$$[Mn_2^{4+}]O_4 + n\mathrm{LiOH} \rightarrow \mathrm{Li}_n[Mn_n^{3+}Mn_{2-n}^{4+}]O_4 + (n/2)H_2O + (n/4)O_2 \quad (2)$$

The XRD patterns after Li sorption were identical to those of the parent compounds, showing the reformation of single-phase products (Figure 7).

The evolutions of the Cr and Mn K-edge XANES spectra of the $x = 0.2$ compound with lithium extraction and reinsertion are shown in Figure 8. Spectra for the $x = 0.5$ compound showed the same behavior. There was no significant change in the Cr absorption edges after the extraction and reinsertion processes, confirming that the Cr ions remaining in the solid are stable in the 16d site and do not participate in the electron transfer process. There was no evidence in the spectra of increased preedge intensity; therefore, any higher oxidation state Cr species which might have formed during acid leaching had been fully removed from the solid. The Mn spectra show a shift of the absorption edge to higher energy after the first delithiation in 0.5 M acid, correlating with oxidation of the Mn ions in the solid to the +4 state. The XANES resonances in the Mn absorption edge also "sharpen up" with lithium extraction due to the removal of contributions from Mn^{3+} ions.[27] The Mn XANES spectra of the compounds after leaching in 0.5 M and 1 M acid were identical, confirming that the additional lithium extraction in more concentrated acid occurred by a mechanism such as Cr leaching rather than by reaction 1. Following lithium sorption from hydroxide solution in the compounds treated with 0.5 M acid, the Mn absorption edges returned to the same position as that of the original parent phases, consistent with the reversibility of the redox process as represented by reaction 2.

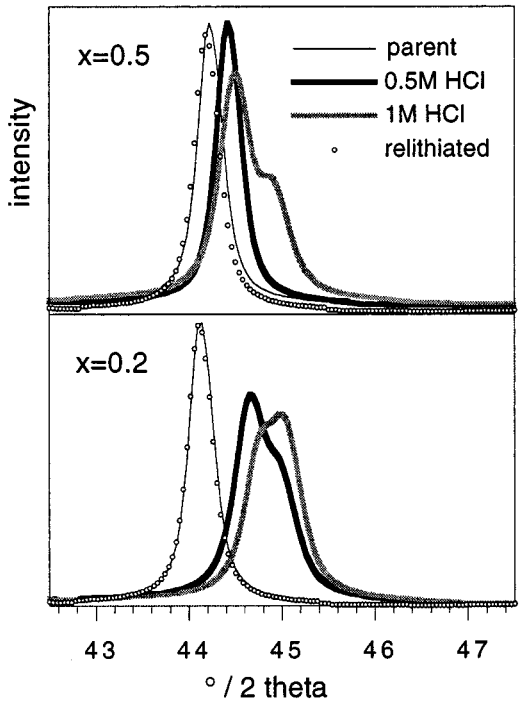

Figure 7. Peak profiles of the [400] reflection in the powder XRD data for the $x = 0.2$ and $x = 0.5$ $LiCr_xMn_{2-x}O_4$ compounds following leaching in 0.5 M HCl and 1 M HCl, and of the 0.5 M HCl-leached compounds after sorption of Li in 0.1 M LiOH.

Structural parameters refined from the EXAFS data for the $x = 0.2$ and $x = 0.5$ spinels after acid leaching and for the 0.5 M HCl-leached sample after reinsertion of Li are given in Table 4. Figure 9 shows the Fourier-transformed EXAFS data at the Cr and Mn edges for the $x = 0.2$ compound. Leaching of lithium in HCl resulted in increased intensities of the Fourier peaks in both the Cr and Mn data. The differences were most significant in the case of Mn, where the Debye−Waller values for the Mn−O and Mn−M shells decreased with acid leaching to values comparable to those for lithium-extracted $LiMn_2O_4$. This can again be attributed to the removal of contributions from Mn^{3+} ions in the lattice. After lithium sorption, the Debye−Waller factors return to the same values as the parent compounds, corresponding to the re-formation of Mn^{3+} ions in the structure.

It may be noted that while both Cr−M and Mn−M distances decrease with Li extraction, a small but increasingly significant difference is observed, with Mn−M distances becoming up to 0.02 Å shorter than Cr−M distances in the same sample. This may be partly related to leaching of Cr ions from the more fully delithiated domains, such that the Cr EXAFS data become

TABLE 4: Structural Parameters from EXAFS of the Cr-Substituted Lithium Manganates Following Leaching in 0.5 M and 1 M HCl, and after Lithium Sorption in LiOH of the Compound Leached in 0.5 M HCl

		Mn−O		Cr−O		Mn−M		Cr−M	
$LiCr_xMn_{2-x}O_4$		R (Å)	σ (Å)	R (Å)	σ (Å)	R (Å)	σ (Å)	R (Å)	σ (Å)
$x = 0.2$	leached 0.5 M HCl	1.908	0.053	1.981	0.036	2.855	0.058	2.869	0.052
	leached 1 M HCl	1.904	0.052	1.981	0.044	2.848	0.059	2.862	0.058
	after Li sorption	1.911	0.072	1.987	0.035	2.894	0.077	2.891	0.052
$x = 0.5$	leached 0.5 M HCl	1.906	0.063	1.977	0.042	2.872	0.057	2.881	0.055
	leached 1 M HCl	1.903	0.054	1.981	0.043	2.856	0.061	2.873	0.056
	after Li sorption	1.906	0.065	1.984	0.045	2.889	0.069	2.891	0.063
$LiMn_2O_4$[a]	lithium-extracted	1.904	0.054			2.841	0.056		
	after Li sorption	1.926	0.074			2.903	0.082		

[a] Parameters taken from ref 27.

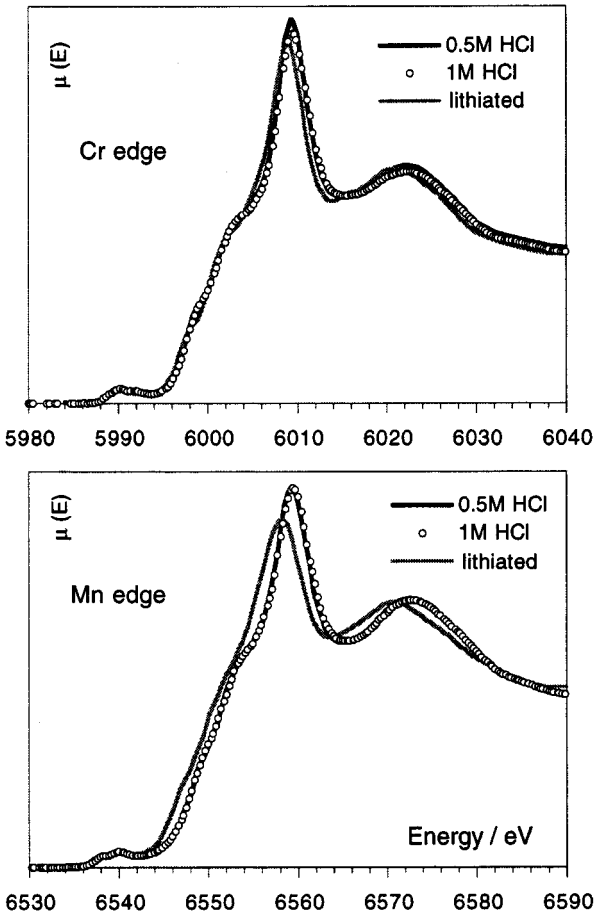

Figure 8. Cr and Mn K-edge XANES spectra of $LiCr_{0.2}Mn_{1.8}O_4$ after leaching in 0.5 M HCl and 1 M HCl, and of the 0.5 M HCl-leached compound after sorption of Li in 0.1 M LiOH.

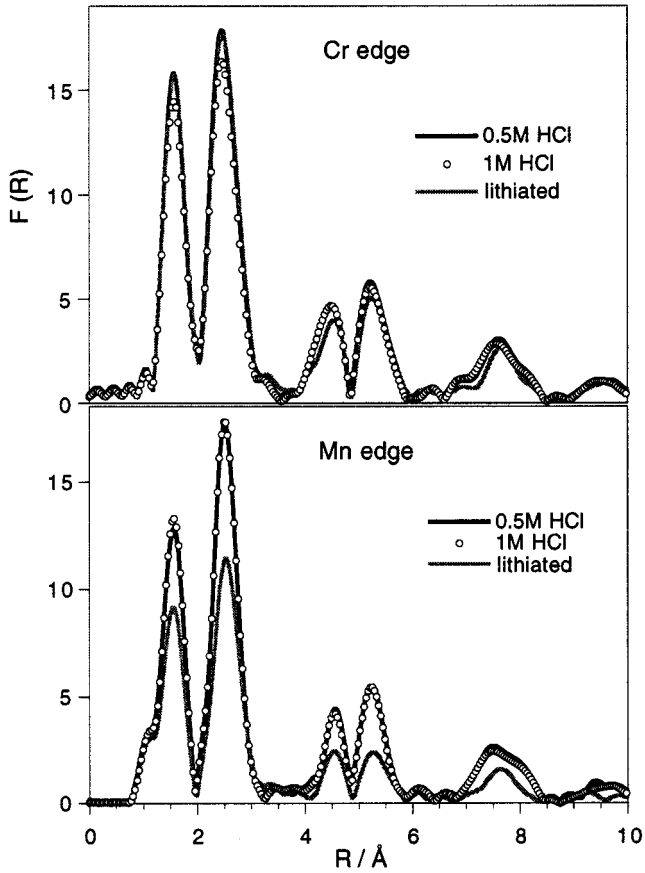

Figure 9. Fourier-transformed Cr and Mn EXAFS data for $LiCr_{0.2}Mn_{1.8}O_4$ after leaching in 0.5 M HCl and 1 M HCl, and of the 0.5 M HCl-leached compound after sorption of Li in 0.1 M LiOH.

increasingly dominated by Cr ions remaining in the less delithiated domains where the lattice is less contracted. However, sorption of Li ions by the compounds leached in 0.5 M HCl resulted in relaxation of the Cr−M and Mn−M distances back to identical values, equivalent to those of the parent compounds, agreeing with the reversibility observed in XRD.

III. Lithium Insertion by Reaction with Butyllithium. The reaction of $LiMn_2O_4$ with butyllithium is known to proceed with insertion of 1 equiv of Li into interstitial sites by reduction of Mn^{4+} ions to Mn^{3+}.[9,20,49] The final $Li_2Mn_2O_4$ product in which all the Mn ions are trivalent is a tetragonal spinel with *I*41/*amd* space group symmetry, but the linkage of edge-sharing $[MnO_6]$ octahedra in the three-dimensional $[Mn_2O_4]$ spinel sublattice is conserved.[13,20] The tetragonal distortion results from the cooperative elongation of the Jahn−Teller $[Mn^{3+}O_6]$ octahedra along the *c* axis of the crystal.

Reaction of the $LiCr_xMn_{2-x}O_4$ compounds with butyllithium produced single-phase tetragonal spinel products as characterized by powder XRD. The compositions of the compounds and the tetragonal unit cell parameters are given in Table 5. As observed for $LiMn_2O_4$,[9] the Cr-substituted spinels incorporated up to 1.2 additional Li ions. While XRD showed a change from cubic to tetragonal crystal symmetry in every case, the tetragonal cell *c*/*a* ratios decrease significantly as the amount of Cr substitution increases. Relating the tetragonal unit cell parameters to those of the precursor cubic phases using $a_C = \sqrt{2}a_T$ and $c_C = a_T$ shows that the degree of tetragonal distortion and the overall expansion of the unit cell volume are both significantly reduced compared with the values of $c/a = 1.16$ and $\Delta V = 5.6\%$ reported for $LiMn_2O_4$.[9,13,20]

The Cr and Mn K-edge XANES spectra of the lithium-inserted $LiCr_xMn_{2-x}O_4$ compounds are compared in Figure 10 for $x = 0.2$ and $x = 1.0$. The spectra at the Mn edge are shifted to lower energy relative to the precursor compounds, while those

TABLE 5: Chemical Compositions and Unit Cell Parameters of the Cr-Substituted Lithium Manganates Following Reaction with Butyllithium

Li_2Cr_x-$Mn_{2-x}O_4$	chemical composition	a_T	c_T	c_C/a_C	ΔV (%)
$x = 0.2$	$Li_{2.21}Cr_{0.23}Mn_{1.77}O_4$	5.69(1)	9.02(1)	1.12	5.6
$x = 0.5$	$Li_{2.14}Cr_{0.51}Mn_{1.49}O_4$	5.72(1)	8.80(2)	1.09	4.6
$x = 1.0$	$Li_{2.09}Cr_{0.98}Mn_{1.02}O_4$	5.79(2)	8.53(3)	1.04	4.0

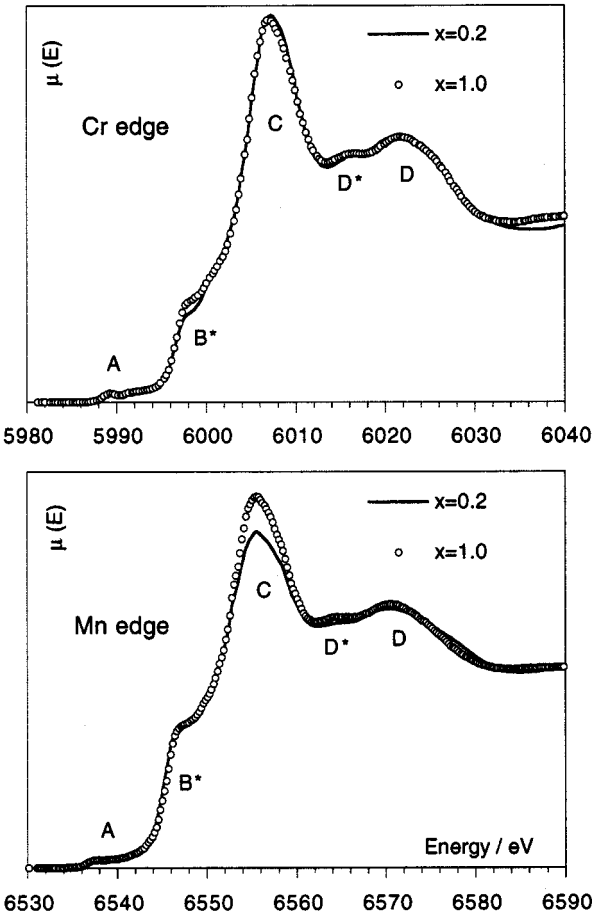

Figure 10. Cr and Mn K-edge XANES spectra of the lithium-inserted $x = 0.2$ and $x = 1.0$ $LiCr_xMn_{2-x}O_4$ compounds.

at the Cr edge remain at the same energy. This is consistent with the electron which accompanies lithium insertion being localized on the Mn ions, but no change occurring in the oxidation state of the trivalent Cr ions. However, the shapes of the XANES were significantly transformed after lithium insertion, with the appearance at both the Cr and Mn edges of a single strong step B*, asymmetric broadening of the resonances C and D, and the appearance of a new resonance D*.

Figure 11 shows the Cr and Mn EXAFS spectra of the lithium-inserted $x = 0.2$ compound, and the Fourier-transformed data for all three compounds are compared in Figure 12. The structural parameters obtained by curve-fitting to the EXAFS data are given in Table 6. Examples of the fits achieved for the $x = 0.5$ compound at the Cr and Mn edges are shown in Figure 13. Although the similarities between the Cr and Mn XANES indicate that the Cr ions remain in the Mn sites, EXAFS shows significant differences between the Cr and Mn local environments, particularly in the first two coordination shells. Excellent fits to the Cr data were obtained by using a single Cr−O distance and a single Cr−M distance, whereas the Mn data required the introduction of two Mn−O distances and two Mn−M distances.

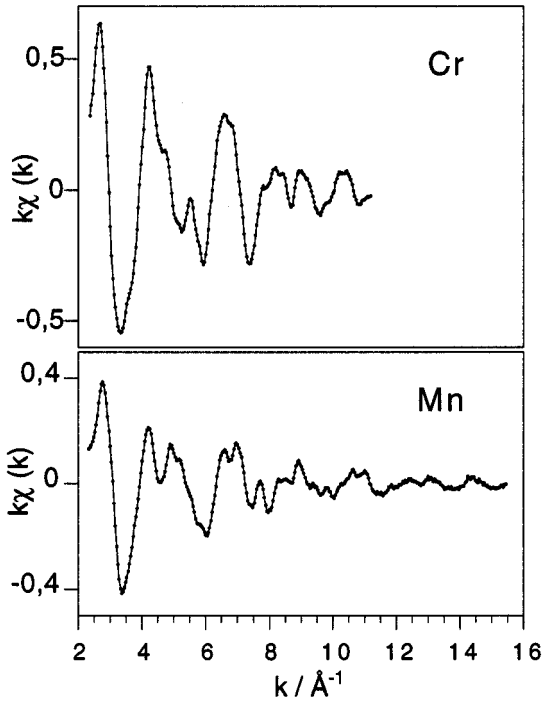

Figure 11. Cr and Mn K-edge EXAFS spectra of $LiCr_{0.2}Mn_{1.8}O_4$ after reaction with butyllithium.

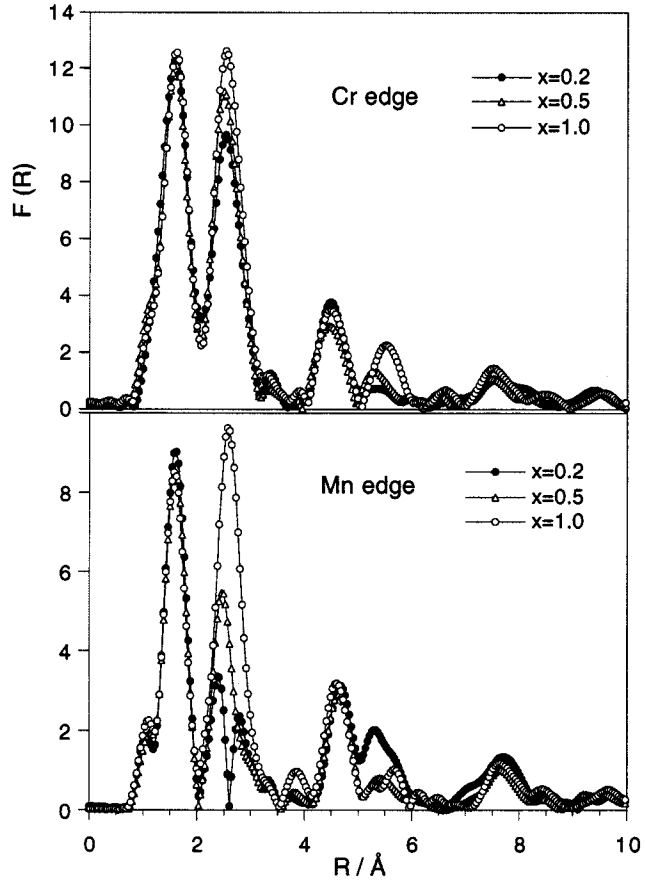

Figure 12. Fourier-transformed Cr and Mn EXAFS data for the $LiCr_xMn_{2-x}O_4$ spinels after reaction with butyllithium.

The EXAFS data show that oxygen atoms retain a regular octahedral coordination around the Cr ions in the tetragonal lattices, and that only around the Mn ions is the octahedral oxygen environment distorted by the Jahn−Teller stabilization of the $[Mn^{3+}O_6]$ cluster. The Cr−O and four short Mn−O

TABLE 6: Structural Parameters from EXAFS for the Cr-Substituted Lithium Manganates Reacted with Butyllithium

	Mn−O		Cr−O		Mn−M		Cr−M	
$Li_2Cr_xMn_{2-x}O_4$	R (Å)	σ (Å)	R (Å)	σ (Å)	R (Å)	σ (Å)	R (Å)	σ (Å)
$x = 0.2$	1.924 (×4)	0.047	1.985 (×6)	0.052	2.825 (×2)	0.058	2.919 (×6)	0.086
	2.25 (×2)	0.123			3.002 (×4)	0.086		
$x = 0.5$	1.925 (×4)	0.050	1.989 (×6)	0.054	2.853 (×2)	0.062	2.915 (×6)	0.078
	2.14 (×2)	0.119			2.988 (×4)	0.091		
$x = 1.0$	1.925 (×4)	0.045	1.988 (×6)	0.050	2.914 (×6)	0.083	2.915 (×6)	0.070
	2.13 (×2)	0.102						

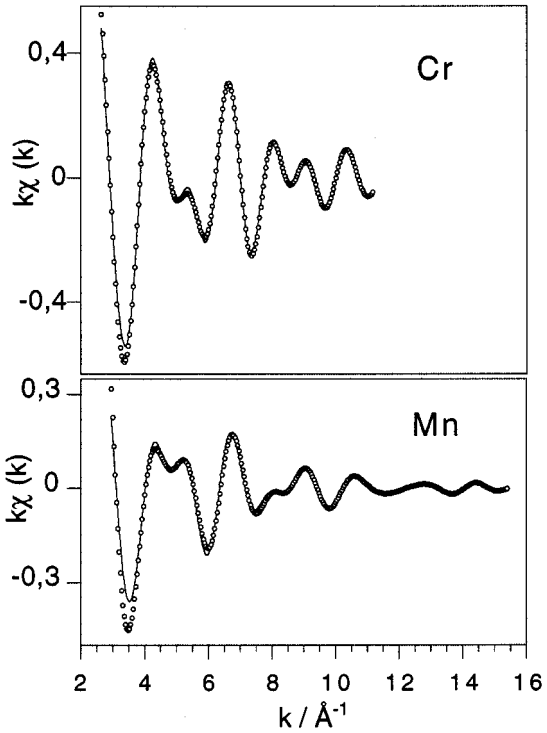

Figure 13. Curve fits (solid lines) to the Cr and Mn EXAFS data (circles) for Li-inserted $LiCr_{0.5}Mn_{1.5}O_4$ filtered over the first two peaks of the Fourier transformations.

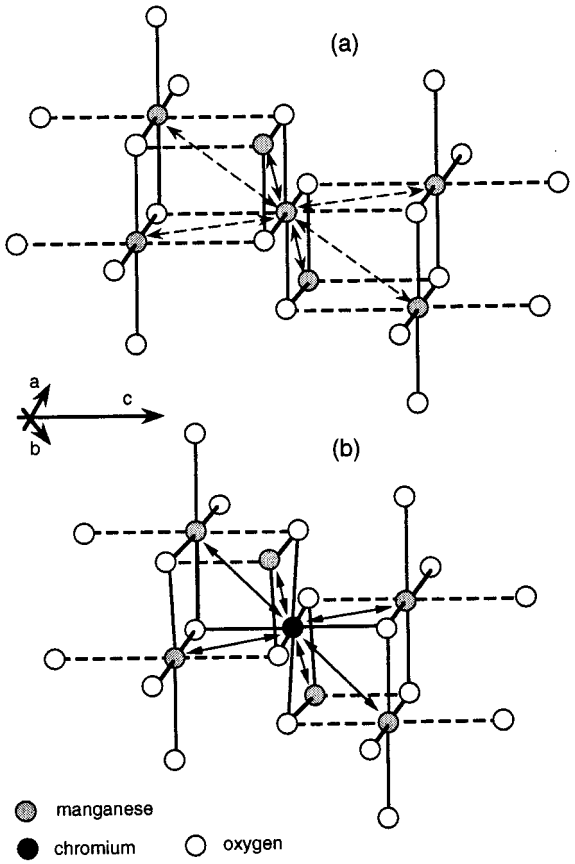

Figure 14. Schematic illustration of the structural effect of a $[CrO_6]$ octahedron in the tetragonal manganese−oxygen spinel framework of $Li_2Mn_2O_4$ formed by Li insertion in $LiMn_2O_4$. (a) In $Li_2Mn_2O_4$, long Mn−O bonds (heavy dashed lines) are oriented along the *c*-axis, while short Mn−O bonds (heavy solid lines) lie in the *a*−*b* plane. Two neighboring Mn ions are at 2.85 Å (thin solid lines) and four Mn ions are at 3.2 Å (thin dashed lines). (b) In the Cr-substituted compounds, Cr−O bonds along the *c*-axis are of equal length to those in the *a*−*b* plane, reducing the displacements of neighboring atoms along the *c*-axis in the local structure.

distances do not vary with changes in the Cr/Mn ratio, but the two long Mn−O distances decrease slightly as the Cr content increases. A recent Rietveld refinement of XRD data for a Li-inserted $LiCrMnO_4$ spinel reported that in the average (Cr,Mn)-O_6 octahedron there were four (Cr,Mn)−O distances of 1.973 Å and two of 2.124 Å.[50] The distances determined here for Cr and Mn indicate that the longer distance belongs to the MnO_6 octahedra only, while the shorter distance would represent an average of oxygen positions in the *a*−*b* plane around Mn and Cr.

There are significant changes in the Fourier peaks corresponding to the cation shells when the Cr/Mn ratio is changed. In the $x = 0.2$ compound, the Mn−M shell is clearly split by the tetragonal distortion of the $[MnO_6]$ octahedron into two subshells at different Mn−M distances. However, as the amount of $[CrO_6]$ in the lattice increases the Mn−M shell becomes increasingly regular. For the $x = 1$ compound, this shell was fitted with six identical Mn−M distances having the same value as that refined for the Cr−M shell.

The structural effect of the $[CrO_6]$ octahedron in the $Li_2Mn_2O_4$ lattice is schematically illustrated in Figure 14. In the absence of Cr, the Mn−Mn coordination shell is split because two neighboring Mn ions lie in the plane of the four short Mn−O bonds (the crystal *a*−*b* plane) giving two short Mn−Mn distances. The other four neighboring Mn ions are displaced to longer Mn−Mn distances by the elongated Mn−O bond. In the Cr-substituted phase, the Cr−O bonds along the *c*-axis are identical to those in the *a*−*b* plane. This inhibits the cooperative displacement of the neighboring cations along the *c*-direction, and therefore reduces the *c*-axis expansion in the local lattice structure. In the Cr EXAFS data there is practically no variation in Cr−M distance between different levels of Cr substitution; the only significant change in the Cr−M shell is a higher Debye−Waller factor when the Cr ions are more dilute in the local structure.

Conclusions

Lithium can be both extracted and inserted in spinel $LiCr_xMn_{2-x}O_4$ compounds. XAFS spectroscopy shows that the substituted Cr forms Cr^{3+} ions at the Mn site and that the Cr ions remain in the trivalent state during processes of lithium

extraction and insertion, except for the highest levels of lithium extraction in acid solution. Since the quantity of lithium which may be reversibly extracted depends mainly on the amount of Mn^{3+} in the compound, Cr substitution lowers the quantity of lithium which can be cycled through the compound in aqueous solutions. Highly substituted compounds are therefore not useful for Li sorption applications. However, small amounts of Cr could be used to prevent lithium extraction from proceeding below the $Li_{0.5}Mn_2O_4$ composition where separation into two phase domains occurs, if this were desirable for a particular application, or to prevent overcharging in lithium batteries. Furthermore, the presence of the electronically stable $[Cr^{3+}O_6]$ octahedra in the spinel framework stabilizes the structure against the local distortions caused by $[Mn^{3+}O_6]$ species. Chromium should therefore improve the structural stability of the compound over multiple extraction−sorption cycles. Chromium substitution will be particularly advantageous for electrochemical applications where loss of $LiMn_2O_4$ electrode capacity is related to the stresses created in the material by large and anisotropic volume changes, most notably when lithium insertion occurs to give $Li_2Cr_xMn_{2-x}O_4$ phases.

Acknowledgment. This work was undertaken as part of a New Zealand Science and Technology Postdoctoral Fellowship awarded to B.A. by the New Zealand Foundation for Research, Science and Technology. Financial support from the French Ministère des Affaires Etrangères through the France-New Zealand Cultural Agreement is also acknowledged with appreciation, and from the New Zealand Ministry of Research, Science and Technology through the Bilateral Research Activities Program (BRAP) for a travel grant to perform XAFS experiments in 1996. The CEA-CNRS-MENESR is thanked for access to the facilities at LURE.

References and Notes

(1) Shen, X.-M.; Clearfield, A. J. *J. Solid State Chem.* **1986**, *64*, 270.
(2) Ooi, K.; Miyai, Y.; Katoh, S. *Sep. Sci. Technol.* **1986**, *21*, 755.
(3) Ooi, K.; Miyai, Y.; Katoh, S. *Sep. Sci. Technol.* **1987**, *22*, 1779.
(4) Leont'eva, G. V.; Chirkova, L. G. *Zh. Prikl. Khim.* **1988**, *61*, 734.
(5) Ooi, K.; Miyai, Y.; Katoh, S.; Maeda, H.; Abe, M. *Langmuir* **1989**, *5*, 150.
(6) Ooi, K.; Miyai, Y.; Sakakihara, J. *Langmuir* **1991**, *7*, 1167.
(7) Feng, Q.; Kanoh, H.; Miyai, Y.; Ooi, K. *Langmuir* **1992**, *8*, 1861.
(8) Kanoh, H.; Ooi, K.; Miyai, Y.; Katoh, S. *Sep. Sci. Technol.* **1993**, *28*, 643.
(9) Thackeray, M. M.; David, W. I. F.; Bruce, P. G.; Goodenough, J. B. *Mater. Res. Bull.* **1983**, *18*, 461.
(10) Thackeray, M. M.; Johnson, P. J.; de Picciotto, L. A.; Bruce, P. G.; Goodenough, J. B. *Mater. Res. Bull.* **1984**, *19*, 179.
(11) Rossouw, M. H.; de Kock, A.; de Picciotto, L. A.; Thackeray, M. M.; David, W. I. F.; Ibberson, R. M. *Mater. Res. Bull.* **1990**, *25*, 173.
(12) de Kock, A.; Rossouw, M. H.; de Picciotto, L. A.; Thackeray, M. M.; David, W. I. F.; Ibberson, R. M. *Mater. Res. Bull.* **1990**, *25*, 657.
(13) Ohzuku, T.; Kitagawa, M.; Hirai, T. *J. Electrochem. Soc.* **1990**, *137*, 769.
(14) Guyomard, D.; Tarascon, J. M. *J. Electrochem. Soc.* **1992**, *139*, 937.
(15) Barker, J.; Koksbang, R.; Saïdi, M. Y. *Solid State Ionics* **1995**, *82*, 143.
(16) Saïdi, M. Y.; Barker, J.; Koksbang, R. *Electrochim. Acta* **1996**, *41*, 199.
(17) Thackeray, M. M.; de Kock, A.; David, W. I. F. *Mater. Res. Bull.* **1993**, *28*, 1041.
(18) Thackeray, M. M.; de Kock, A.; Rossouw, M. H.; Liles, D. C.; Bittihn, R.; Hoge, D. *J. Electrochem. Soc.* **1992**, *139*, 363.
(19) Le Cras, F.; Strobel, P.; Anne, M.; Bloch, D.; Soupart, J.-P.; Rousche, J.-C. *Eur. J. Solid State Inorg. Chem.* **1996**, *33*, 67.
(20) Mosbah, A.; Verbaère, A.; Tournoux, M. *Mater. Res. Bull.* **1983**, *18*, 1375.
(21) Tarascon, J. M.; McKinnon, W. R.; Coowar, F.; Bowmer, T. N.; Amatucci, G.; Guyomard, D. *J. Electrochem. Soc.* **1994**, *141*, 1421.
(22) Takada, T.; Hayakawa, H.; Akiba, E. *J. Solid State Chem.* **1995**, *115*, 420.
(23) Yamada, A.; Miura, K.; Hinokuma, K.; Tanaka, M. *J. Electrochem. Soc.* **1995**, *142*, 2149.
(24) Gao, Y.; Reimers, J. N.; Dahn, J. R. *Phys. Rev. B* **1996**, *54*, 3878.
(25) Ammundsen, B.; Burns, G. R.; Jones, D. J.; Rozière, J. *Chem. Mater.* **1995**, *7*, 2151.
(26) Ammundsen, B.; Aitchison, P. B.; Burns, G. R.; Jones, D. J.; Rozière, J. *Solid State Ionics* **1997**, *97*, 269.
(27) Ammundsen, B.; Burns, G. R.; Jones, D. J.; Rozière, J. *Chem. Mater.* **1996**, *8*, 2799.
(28) Ammundsen, B.; Rozière, J.; Islam, M. S. *J. Phys. Chem. B* **1997**, *101*, 8156.
(29) Sato, K.; Poojary, D. M.; Clearfield, A.; Kohno, M.; Inoue, Y. *J. Solid State Chem.* **1997**, *131*, 84.
(30) Tarascon, J. M.; Wang, E.; Shokoohi, F. K.; McKinnon, W. R.; Colson, S. *J. Electrochem. Soc.* **1991**, *138*, 2859.
(31) Suzuki, S.; Tomita, M.; Okada, S.; Arai, H. *J. Phys. Chem. Solids* **1996**, *57*, 1851.
(32) Pistoia, G.; Antonini, A.; Rosati, R.; Bellitto, C.; Ingo, G. M. *Chem. Mater.* **1997**, *9*, 1443.
(33) Guohua, L.; Ikuta, H.; Uchida, T.; Wakihara, M. *J. Electrochem. Soc.* **1996**, *143*, 178.
(34) Baochen, W.; Yongyao, X.; Li, F.; Dongjiang, Z. *J. Power Sources* **1993**, *43*−*44*, 539.
(35) Appetecchi, G. B.; Scrosati, B. *J. Electrochem. Soc.* **1997**, *144*, L138.
(36) Sigala, C.; Guyomard, D.; Verbaere, A.; Piffard, Y.; Tournoux, M. *Solid State Ionics* **1995**, *81*, 167.
(37) Pistoia, G.; Wang, G.; Wang, C. *Solid State Ionics* **1992**, *58*, 285.
(38) Wakihara, M.; Guohua, L.; Ikuta, H.; Uchida, T. *Solid State Ionics* **1996**, *86*−*88*, 907.
(39) Hunter, J. C. *J. Solid State Chem.* **1981**, *39*, 142.
(40) Ammundsen, B.; Jones, D. J.; Rozière, J. *J. Phys. IV* **1997**, *7*, 1257.
(41) Wilhelmi, K. *Acta Chem. Scand.* **1968**, *22*, 2565.
(42) Rodriguez-Carvajal, J. Internal Report, Institut Laue-Langevin, France.
(43) Michalowicz, A. In *Logiciels pour la Chimie*; Société Française de Chimie: Paris, 1991; p 102.
(44) Zabinsky, S. I.; Rehr, J. J.; Ankudinov, A.; Albers, R. C.; Eller, M. J. *Phys. Rev. B* **1995**, *52*, 2995.
(45) Farges, F.; Brown Jr., G. E.; Rehr, J. J. *Geochim. Cosmochim. Act.* **1996**, *60*, 3023.
(46) (a) Durham, P. J.; Pendry, J. B.; Hodges, C. H. *Solid State Commun.* **1981**, *38*, 159. (b) Sainctavit, P.; Petiau, J.; Benfatto, M.; Natoli, C. R. *Phys. B* **1989**, *158*, 347.
(47) Ammundsen, B.; Jones, D. J.; Rozière, J.; Berg, H.; Tellgren, R.; Thomas, J. O. *Chem. Mater.* **1998**, *10*, 1680.
(48) (a) Manceau, A.; Charlet, L. *J. Colloid Interface Sci.* **1992**, *148*, 425. (b) Silvester, E.; Charlet, L.; Manceau, A. *J. Phys. Chem.* **1995**, *99*, 16662.
(49) David, W. I. F.; Thackeray, M. M.; de Picciotto, L. A.; Goodenough, J. B. *J. Solid State Chem.* **1987**, *67*, 316.
(50) Kano, S.; Sato, M. *Solid State Ionics* **1995**, *79*, 215.